

Electron microscopy study of yttrium doped $\text{Ba}_{0.5}\text{Sr}_{0.5}\text{Co}_{0.8}\text{Fe}_{0.2}\text{O}_{3-\delta}$

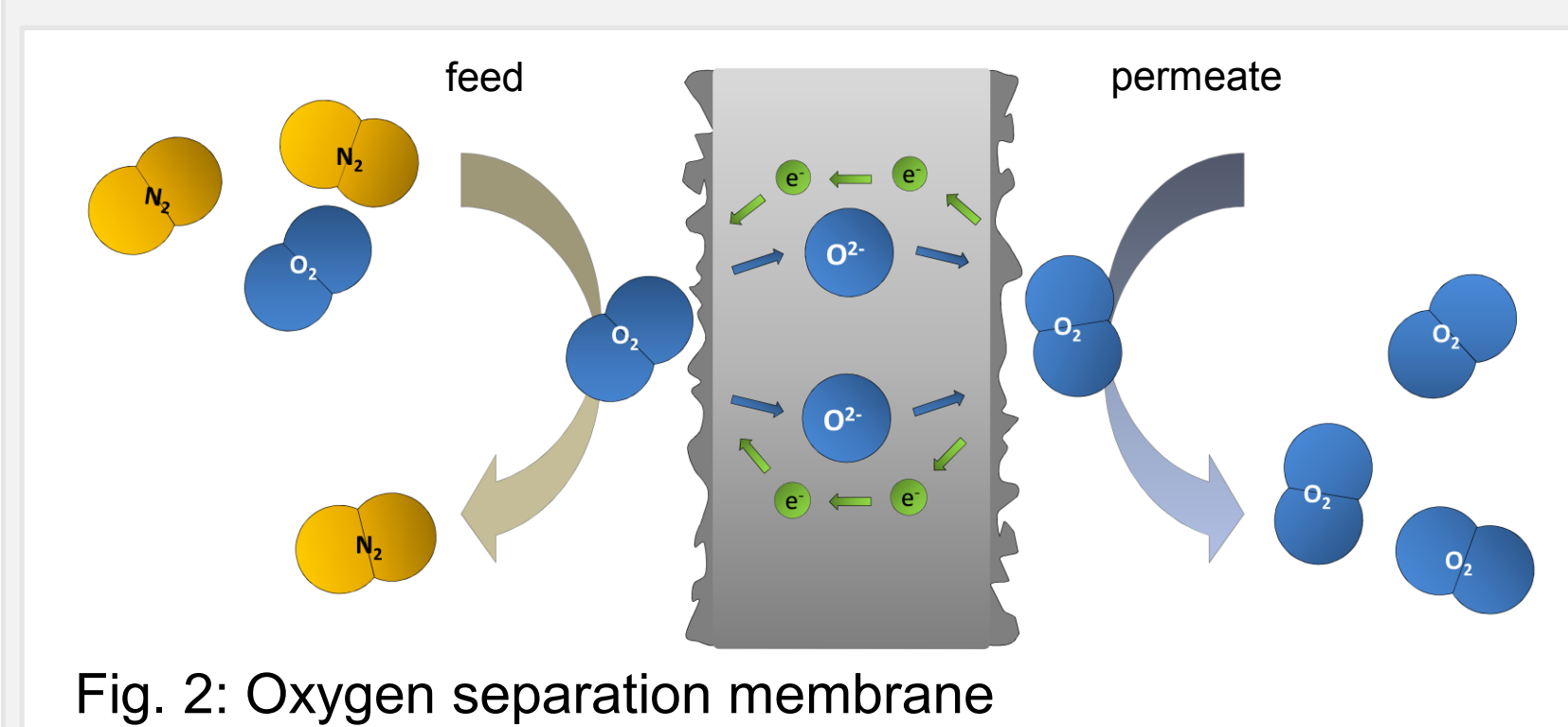
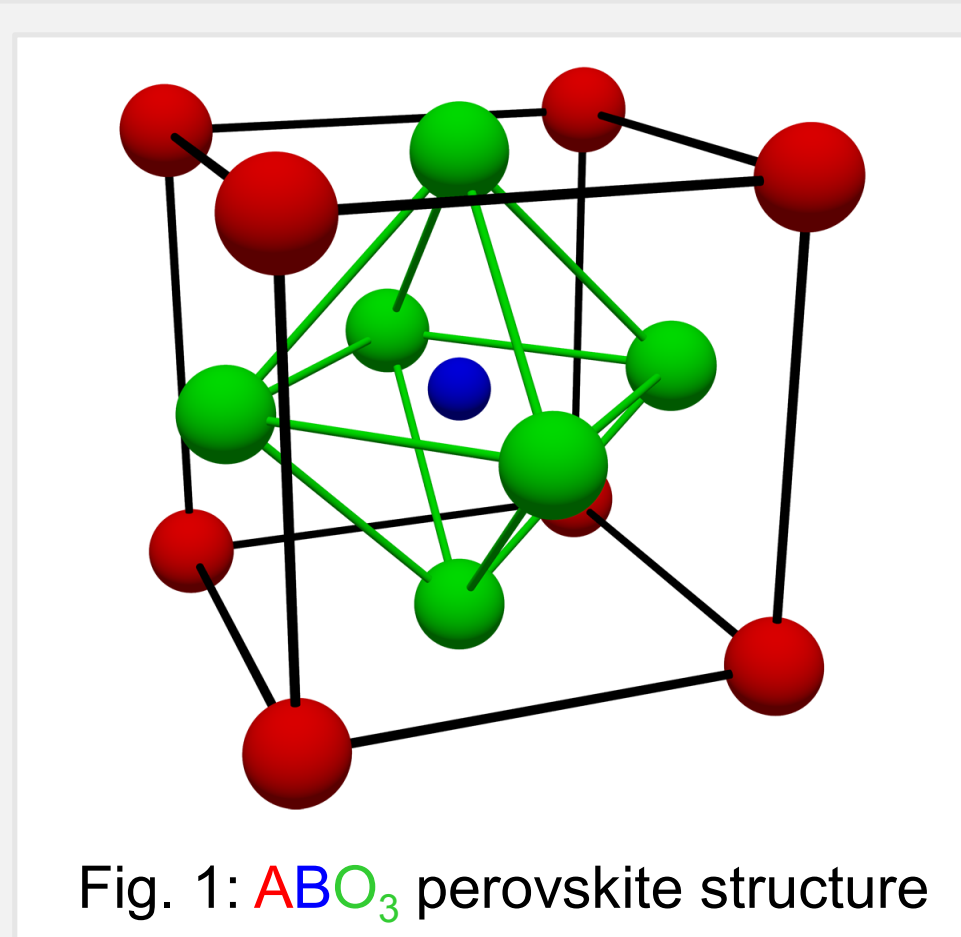
M. Meffert^{1,3}, P. Müller^{1,3}, H. Störmer¹, C. Niedrig², S. F. Wagner², E. Ivers-Tiffée^{2,3}, D. Gerthsen^{1,3}

1. Laboratory for Electron Microscopy (LEM), Karlsruhe Institute of Technology (KIT), 76131 Karlsruhe/Germany
 2. Institut für Werkstoffe der Elektrotechnik (IWE), Karlsruhe Institute of Technology (KIT), 76131 Karlsruhe/Germany
 3. DFG Center for Functional Nanostructures (CFN), Karlsruhe Institute of Technology (KIT), 76131 Karlsruhe/Germany

Contact: matthias.meffert@kit.edu

Introduction

- $\text{Ba}_{0.5}\text{Sr}_{0.5}\text{Co}_{0.8}\text{Fe}_{0.2}\text{O}_{3-\delta}$ (BSCF) in the cubic phase promising mixed ionic and electronic conducting perovskite (Fig. 1)
- Application in future CO_2 -emission free power plants as oxygen separation membrane (Fig. 2)
- Highest oxygen conductivity at application relevant temperatures (700 ... 900 °C)
- However, *fast degradation and poor long time stability at temperatures below 900 °C* by secondary phase formation (hexagonal BSCF, CoO , „plate-like“ precipitates [1,2] consisting of lamellae of different phases (cubic, hexagonal and Ba-cobaltate) induced by temperature-dependent change of O-concentration and corresponding change of Co-valence state
- Improvement of conductivity and stability through B-site doping with monovalent transition metals [3, 4]



- Scanning electron microscopy (SEM) and additional Transmission electron microscopy (TEM) investigations reveal decomposition process and phase stability

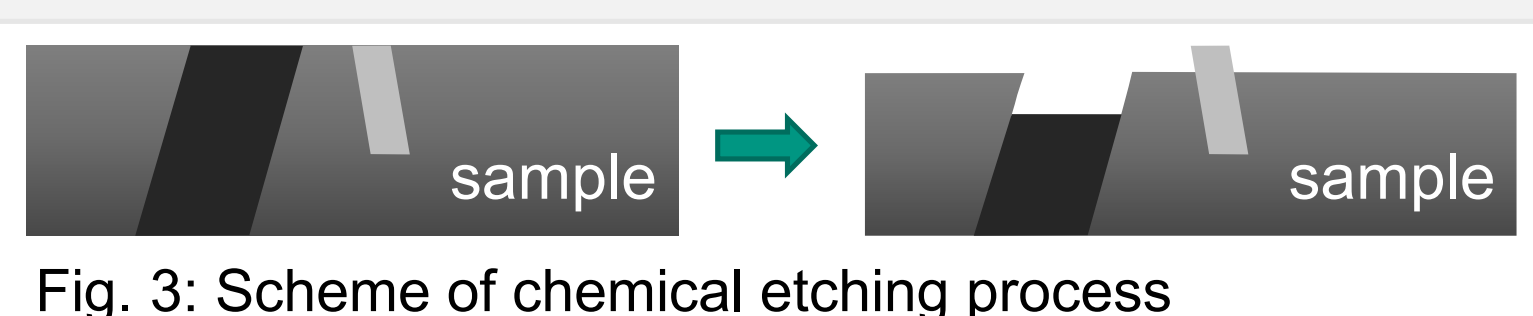
Fabrication

- Calcination of powder by mixed oxide route
- Dopant concentration: 0 – 10 at% Y on B-site
- Isostatic pressing at 250 MPa into ceramic compacts
- Sintering at 1100 °C for 12 h and homogenization at 1000 °C for 24 h
- Annealing in air at 700 – 900 °C for 100 h and quenching in water

Sample preparation

SEM sample preparation and phase mapping

- Polishing by diamond lapping film
- Chemical etching using colloidal silicon (Fig. 3)
- SEM imaging in ZEISS LEO 1530 Gemini and FEI Quanta 650 ESEM



- ➔ Contrast due to topography
- ➔ Mapping of different phases by SEM imaging [1] (Fig. 4)

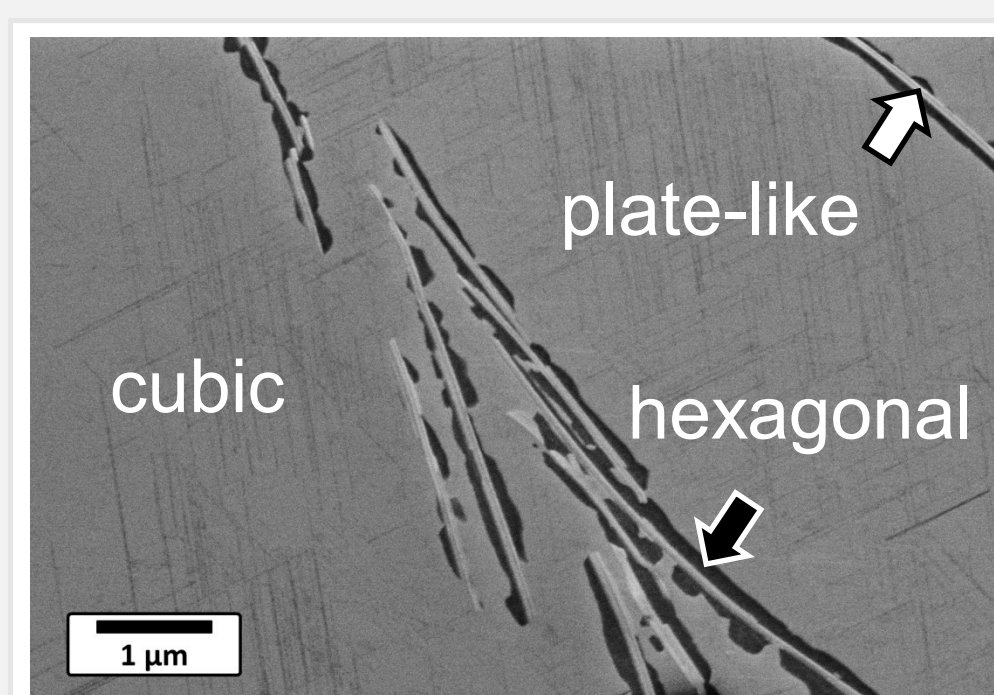


Fig. 4: SEM image of chemically etched BSCF bulk

TEM, STEM, EDXS and EELS

- Standard TEM sample preparation by embedding in ceramic cylinder, dimple grinding, Ar^+ -ion milling
- Microscopes: Philips CM 200 FEG/ST and FEI Titan³ 80-300

Experimental Results

Microstructure

Yttrium doping suppresses

- CoO precipitates
- Plate-like phase at doping concentrations ≥ 3 at% (Fig. 5)
- ➔ No secondary phases at $T \geq 900$ °C

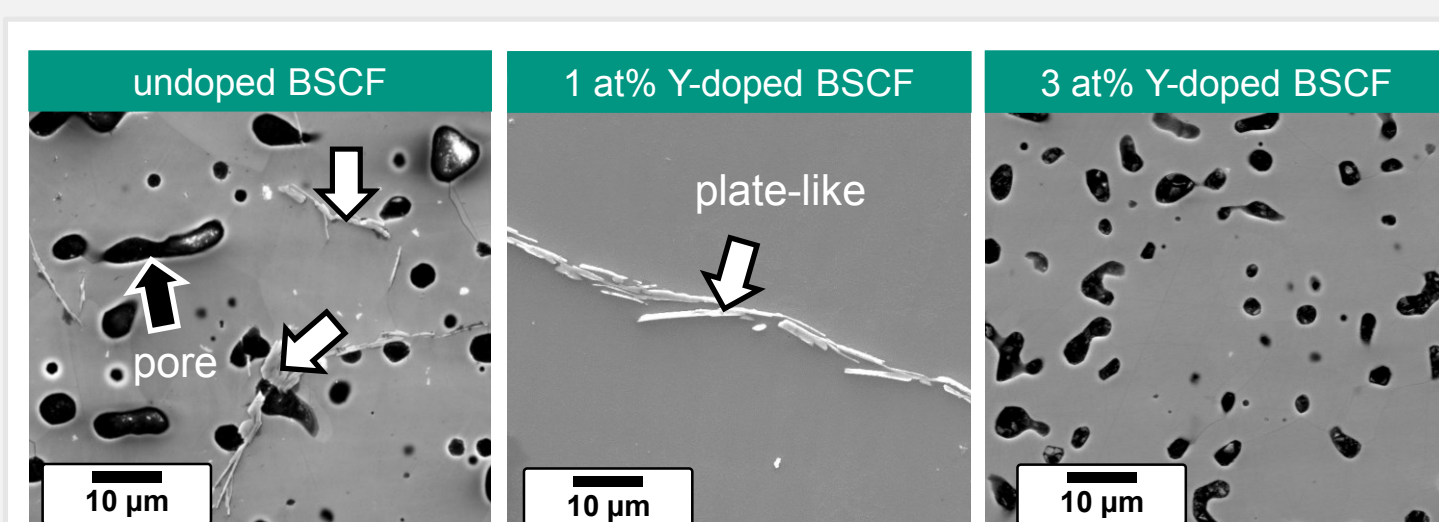


Fig. 5: SEM image of undoped, 1 at% and 3 at% Y doped BSCF annealed at 900 °C for 100 h

References

- [1] P. Müller *et al.*, Solid State Ionics **206** (2012) p. 57.
- [2] P. Müller *et al.*, Chem. Mater. **24** (2013) p. 564.
- [3] S. Yakovlev *et al.*, Appl. Phys. Lett. **96** (2010) p. 254101.
- [4] P. Haworth *et al.*, Sep. Purif. Technol. **81** (2011) p. 88.

- Formation of hexagonal phase at grain boundary triple points (Fig. 5)
- Increasing decoration of grain boundaries at lower temperatures ($T < 800$ °C)

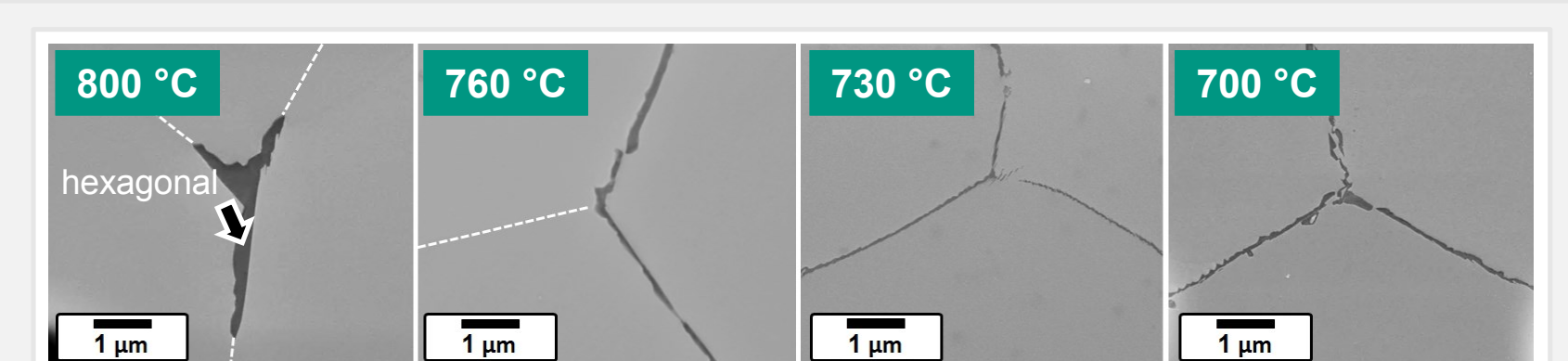


Fig. 6: SEM images of hexagonal phase at different annealing temperatures of 3 at% Y-doped BSCF

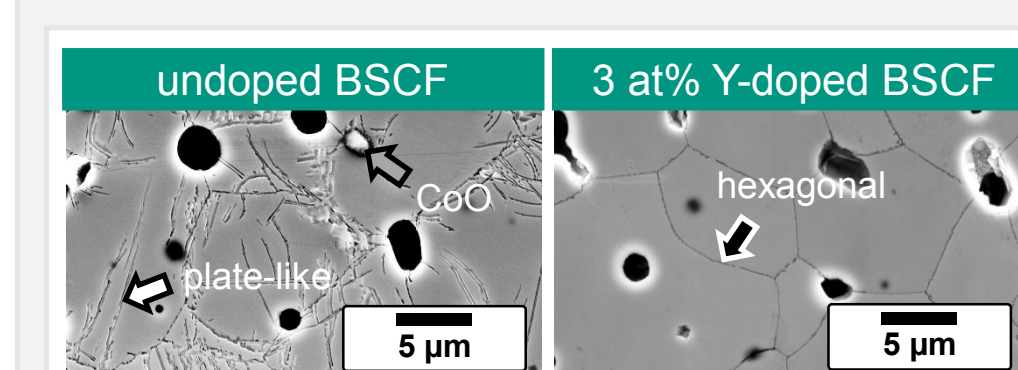


Fig. 7: SEM images of doped and undoped BSCF annealed at 700 °C for 100 h

But: Significant reduction of volume fraction of secondary phases (Fig. 7)

- Hexagonal phase Co-rich, Fe- and Y-depleted (Fig. 8)
- Minor deviation in Ba- and Sr-concentration

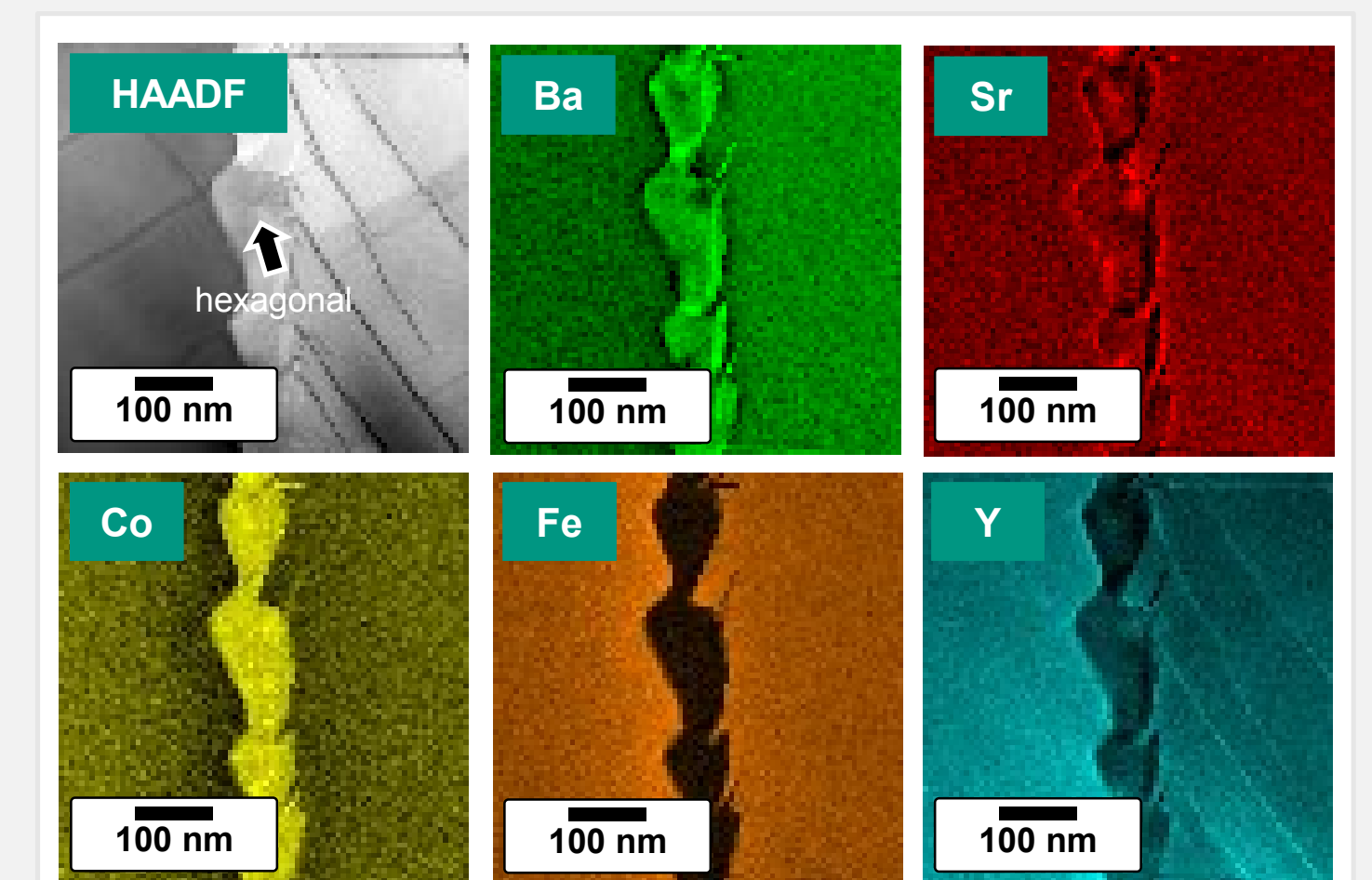


Fig. 8: HAADF-STEM image and EDXS mapping of 3 at% Y-doped BSCF annealed at 700 °C

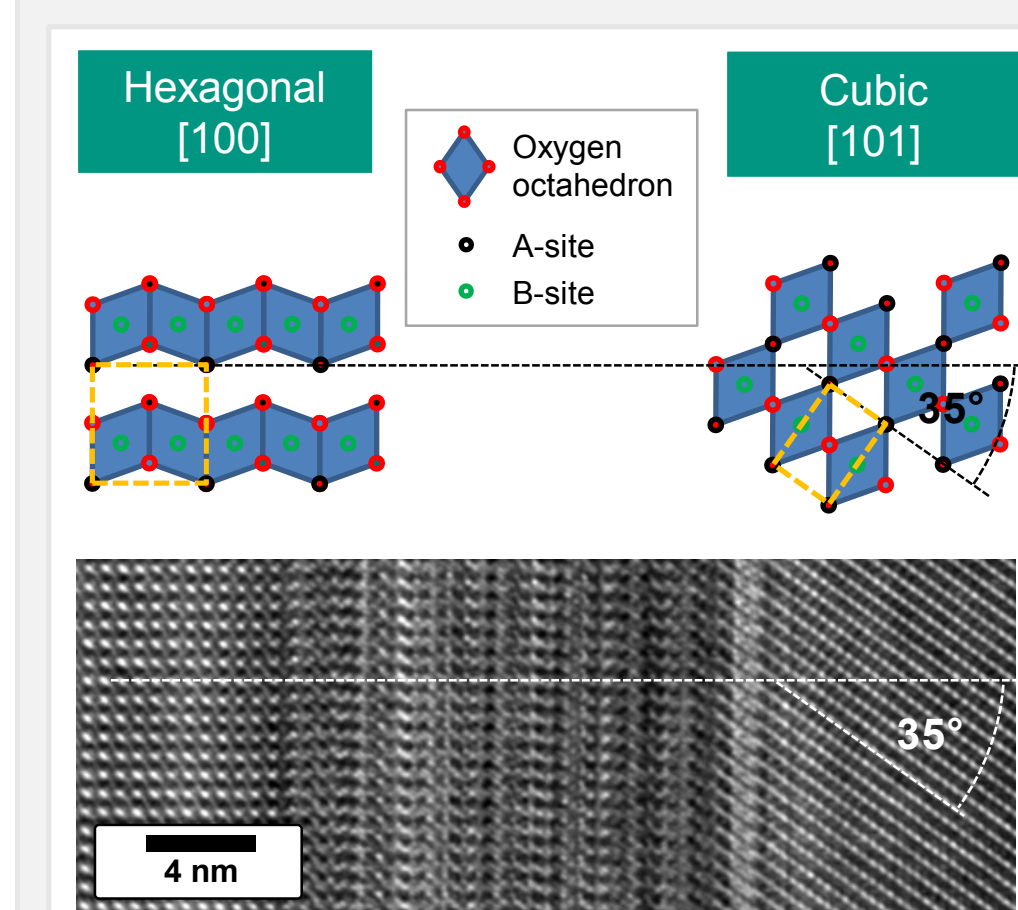


Fig. 9: HRTEM image of interface region between hexagonal and cubic phase

- Orientation relationship between cubic and hexagonal phase
- ➔ Configuration change of oxygen octahedrons from corner-sharing (cubic) to face-sharing (hexagonal) (Fig. 9)
- Complex arrangement of lamellae consisting of cubic and hexagonal phase at interface region (Fig. 9)

Co-valence determination in the cubic and hexagonal BSCF phase

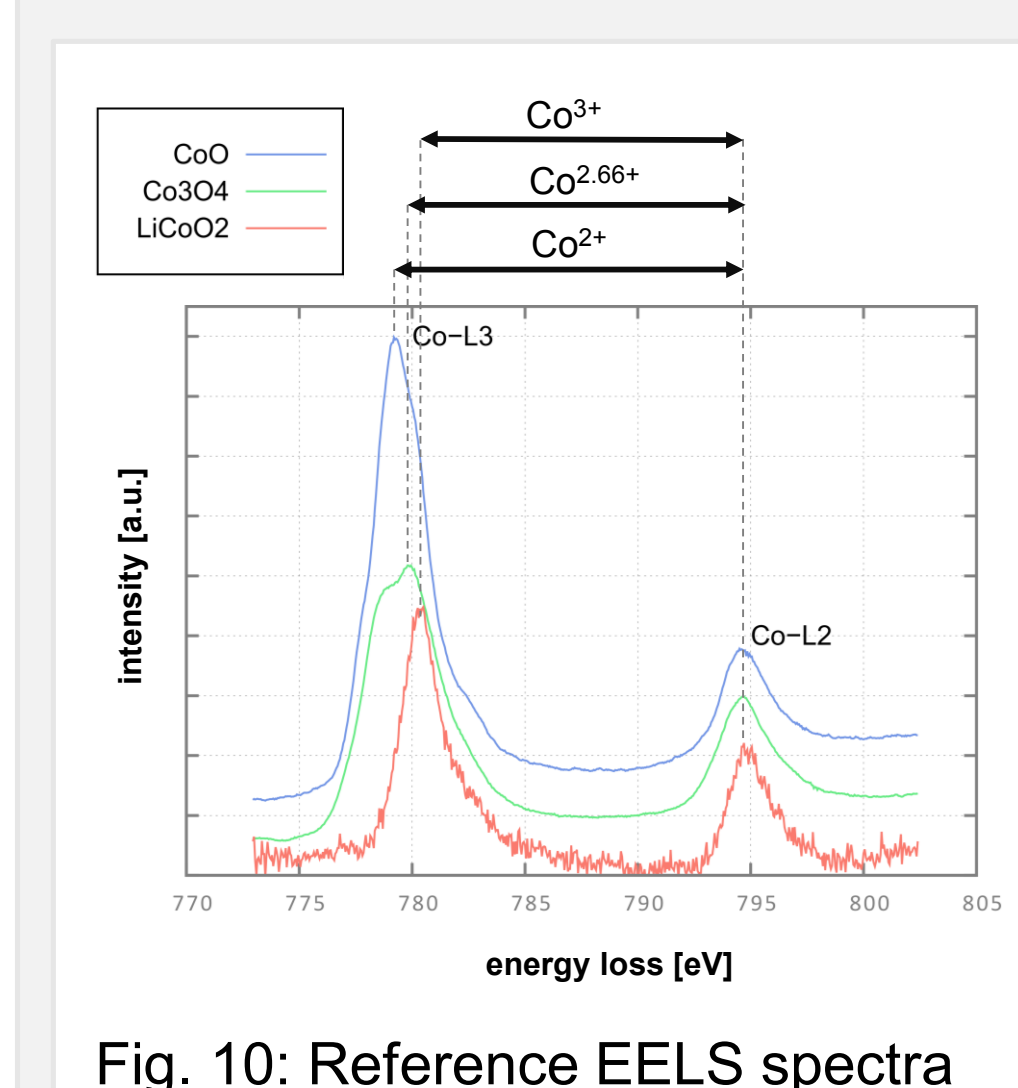


Fig. 10: Reference EELS spectra

- Correlation between $\text{Co-L}_2/\text{L}_3$ white-line distance and valence according to reference samples with known Co-valence (Fig. 10)
- Noise reduction of spectra by principle component analysis
- ➔ *Fast valence-state mapping of BSCF on the basis of L_2/L_3 white-line distance*

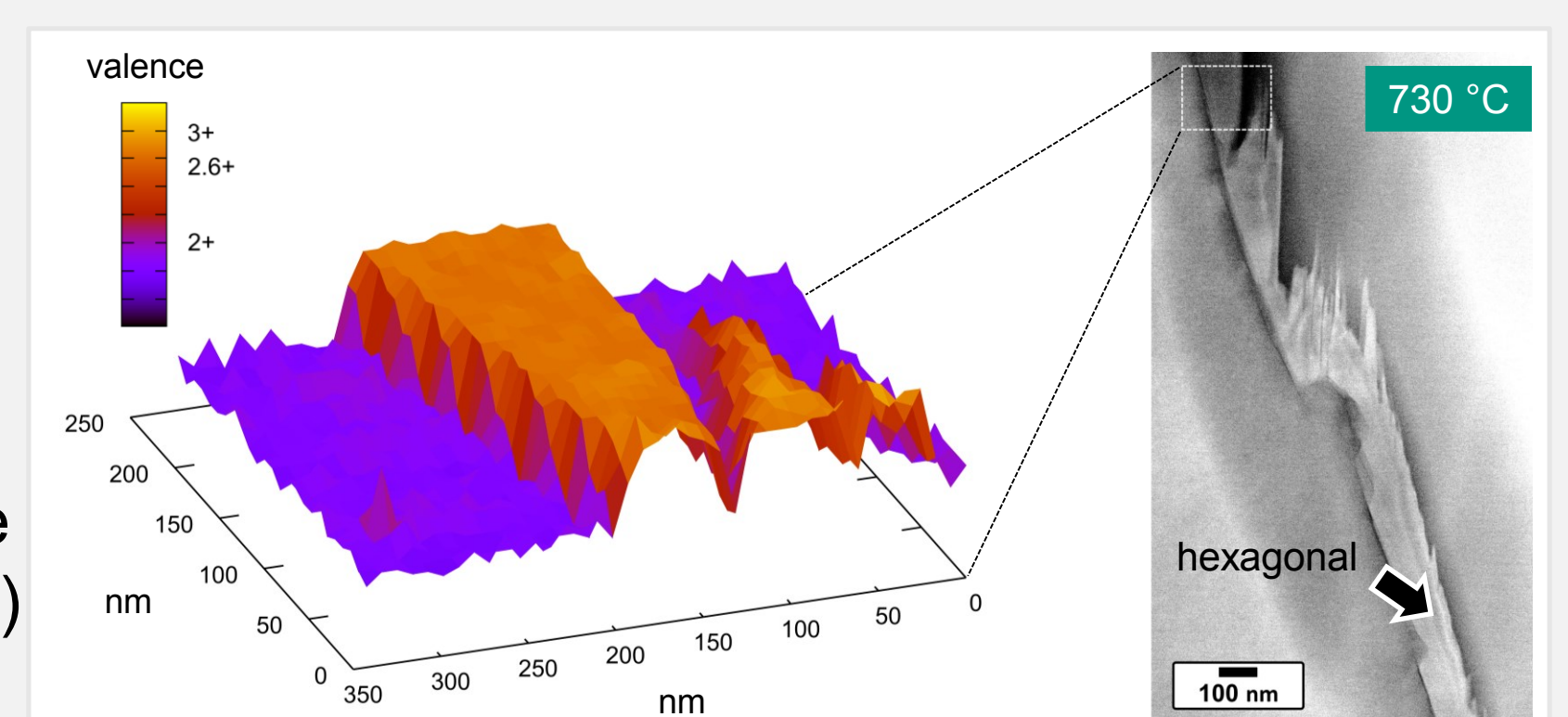


Fig. 11: Co-valence mapping of 3 at% Y-doped BSCF

- Change of average valence from 2.0 ± 0.3 (cubic BSCF) to 2.6 ± 0.3 (hexagonal BSCF) (Fig. 11)

Summary

- Y-doping suppresses plate-like phase and CoO precipitates (Fig. 12) and confines hexagonal phase to grain boundaries
- New fast EELS-based technique for Co-valence state mapping by correlation of $\text{Co-L}_2/\text{L}_3$ white-line distance and Co-valence state for valences between 2+ and 3+

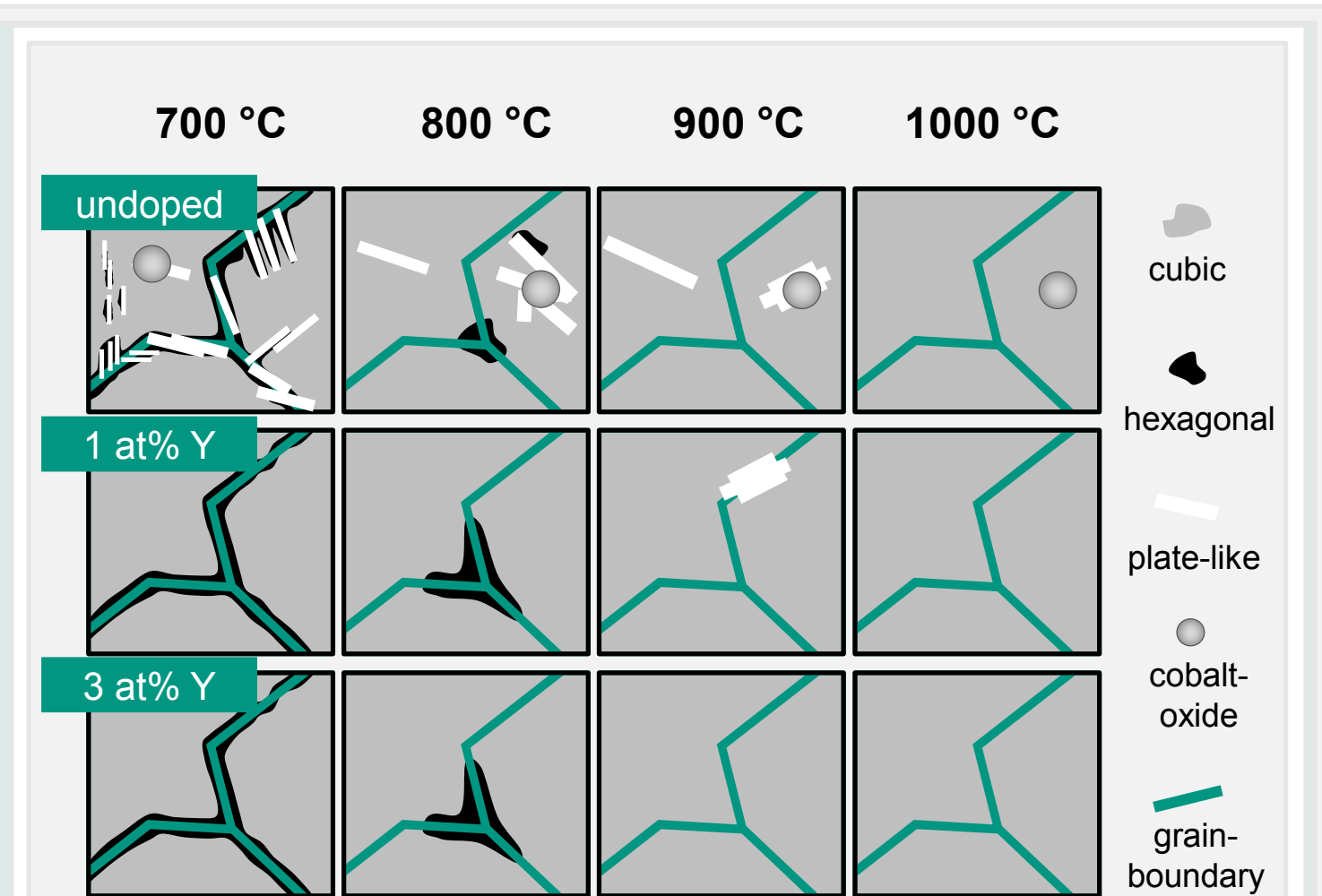


Fig. 12: Schematics of microstructure

Acknowledgement

This work has been performed within the project F.2 of the DFG Research Center for Functional Nanostructures (CFN). It has been further supported by a grant from the Ministry of Science, Research and the Arts of Baden-Württemberg (Az: 7713.14-300) and by the Helmholtz Association of German Research Centres through the portfolio topic MEM-BRAIN.